Check for updates

Tuning Composition of Multicomponent Surface Nanodroplets in a Continuous Flow-In System

*Jae Bem You, Detlef Lohse, and Xuehua Zhang**

Droplets are excellent platforms for compartmentalization of many processes such as chemical reactions, liquid–liquid extraction, and biological or chemical analyses. Accurately controlling and optimizing the composition of these droplets is of high importance to maximize their functionality. In this work, the formation of multicomponent droplets with controllable composition by employing a continuous flow-in setup is demonstrated. Multiple streams of different oil solutions are introduced and mixed in a passive flow mixer and the outcoming mixture is subsequently fed into a flow chamber to form surface nanodroplets by solvent exchange. This method is time-effective, enabling programmable continuous processes for droplet formation and surface cleaning. The surface nanodroplets are formed within 2.5 min in one cycle, and the droplet formation is reliable with similar size distribution over multiple cycles. The composition of the resulting surface nanodroplet can be tuned at will simply by controlling the flow rate ratios of each stream of the oil solution. Using fluorescence imaging, it is shown that the composition of the binary surface nanodroplets agrees well with theoretical values predicted using the phase diagram.

1. Introduction

Droplets have been regarded as platforms for compartmentalization of many processes in chemical reactions,[1–3] liquid–liquid extractions,[4,5] biological analysis,[6,7] pharmaceuticals,[8] analyte detection,[9,10] novel material synthesis,[11–13] among many others. The high surface area-to-volume ratio of microdroplets enables rapid materials exchange across the droplet-liquid interface that

J. B. You,[+] X. Zhang
Department of Chemical and Materials Engineering
University of Alberta
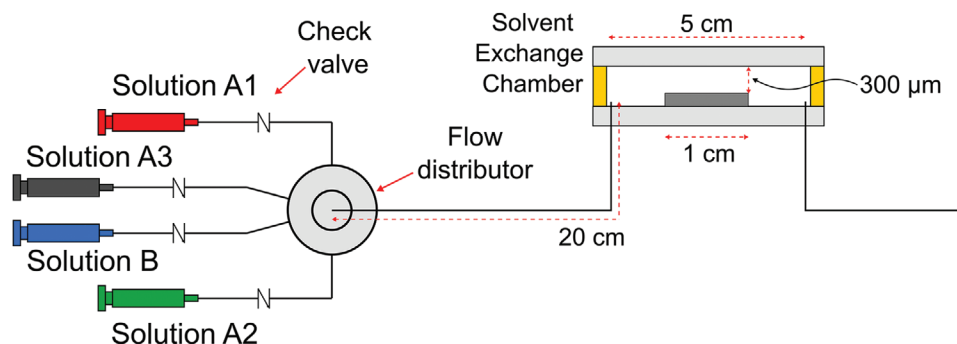Alberta T6G 1H9, Canada
E-mail: xuehua.zhang@ualberta.ca
J. B. You, D. Lohse, X. Zhang
Physics of Fluids Group, Max Planck Center Twente
for Complex Fluid Dynamics
JM Burgers Center for Fluid Dynamics, Mesa+
Department of Science and Technology
University of Twente
Enschede 7522 NB, The Netherlands

[+]Present address: Department of Chemical Engineering, Kyungpook National University, Daegu, 41566 Republic of Korea

can be leveraged for speeding up chemical reactions,[14] concentrating chemicals from a sample based on partition coefficients.[15] Surface nanodroplets are femtoliter-scale droplets, with a height ranging from ≈5–1000 nm, formed on a target substrate.[16,17] The small volume and pinning effect around their boundary provide the stability of surface nanodroplets under the shear from the flow of an analyte or reactant solution, making surface nanodroplets suitable for rapid microextraction[18] and droplet reactions[19] in continuous flow-in systems. Recent advances in machine learning based methods may lead to rapid and automated droplet generation to establish training data for understanding dynamics of droplets consisting of complex media,[20] reaction kinetics in droplets,[21] and droplet based quantification and determination of chemical species.[22]

In a variety of applications, the composition of multicomponent droplets is required to be optimized in order to achieve the desired functionality and performance of droplets. For example, in liquid–liquid extraction of chemical compounds from liquid solutions, binary droplets consisting of two solvents are used for the extraction performance which depends on the droplet composition because the solubility of a compound is different for every extractant. Binary organic droplets can be excellent media for efficient extraction of organic pollutants or drug compounds with different polarity from aqueous media at once.[23–25] Zhu et al.[23] used binary droplets of methylene chloride and *n*-hexane to extract and detect polycyclic aromatic hydrocarbons from environmental water samples down to a concentration of 2.1 ng L^{-1}. Wang et al.[24] reported that the extraction efficiency of nicotine and cotinidine from urine sample was maximized when undecanol-chloroform binary droplets were used at a volumetric ratio of 1:1 with average recoveries of 91.5% and 79% for nicotine and cotinine, respectively. On the other hand, when only undecanol was used, the extraction efficiency for cotinine was less than 10% while the efficiency for nicotine reached 90%. This shows the strong influence of extractant type on the extraction performance. Thus, reliable formation of multicomponent droplets with optimized droplet composition is of high importance.

Evaporation of deposited drops may be a simple approach leading to formation of nanodroplets on surfaces. However, different compounds in a droplet may lead to selective evaporation of more volatile liquid and complicated transport phenomena due to gradients in surface tension or chemical

Figure 1. Schematic showing the continuous mixing setup for the formation of surface nanodroplets.

concentration.[26–28] For similar reasons, formation of multicomponent nanodroplets may be also challenging for condensation, although it is a simple approach producing nanoscale droplets of single component.[29,30] Multicomponent droplets can also be formed continuously using microfluidic devices in which an inner, dispersed organic (or aqueous) phase is sheared by an outer, continuous aqueous (or organic) phase.[31–33] The composition of the droplets can be controlled by combining multiple streams of dispersed phases into a single mixture stream before shearing it with the continuous phase. However, due to the low Reynolds number and small dimension of droplets, mixing is predominantly driven by diffusion.[34,35] As a result, additional mixing units need to be designed into the microfluidic device to induce chaotic flow inside the droplets to ensure complete mixing between the various components.[3,35]

Recently, the solvent exchange method has been developed as a simple bottom-up approach to produce surface nanodroplets with various compositions.[36–38] In analogy, the droplet formation in the bulk mixtures is known as ouzo effect.[39,40] In the solvent exchange process, a one-phase ternary mixture of a good solvent, a poor solvent and an oil is replaced by the fresh poor solvent. Mixing between the ternary mixture and the fresh poor solvent leads to oil oversaturation and oil droplets nucleate and grow on the target substrate.[36] The formation of the surface nanodroplets can be controlled by tuning parameters such as solution flow rate and chamber height. Most importantly, the droplet composition can be varied by simply tuning the composition of a pre-made ternary mixture.[9,37,41] For instance, Li et al.[9] used a pre-made ternary solution containing two oils, namely 1-octanol and α-tocopherol to form binary droplets which were applied to ultrasensitive sensing of contaminants from water. The α-tocopherol was used to form silver nanoparticles while the 1-octanol in the droplets were responsible for extracting the contaminant molecules from the aqueous sample. As a result, the silver nanoparticles could be used as substrates for surface-enhanced Raman spectroscopy (SERS) for the analysis of extracted contaminants.[9] The flow-in process during the solvent exchange allows for automated droplet formation and optimization of the droplet composition by controlling the solution supply.

In this work, we demonstrate in situ control of multicomponent droplet composition by employing a continuous mixing of various oils during solvent exchange using a continuous flow-in system. Streams of solution A_i (i = 1, 2, and 3) consisting of oils, namely octanol, decane, and toluene in ethanol are mixed

while flowing through a static mixer and the mixture is introduced into the solvent exchange chamber. Subsequently, a poor solvent common to the three oils is introduced to induce the nucleation and growth of multicomponent droplets containing octanol, decane, and toluene. The continuous mixing setup enables reliable droplet formation over repeated cycles, demonstrating its potential application for rapid data acquisition via an automated setup. The composition of the multicomponent droplets can be controlled in situ simply by changing the ratio of flow rates of the different solution A_i. The compositions of the multicomponent droplets, estimated using solvatochromic Nile red fluorescent dye, are in excellent agreement with the theoretical calculations obtained from the ternary phase diagram. This fast and simple approach for producing multicomponent surface nanodroplets with tuneable compositions may provide a powerful platform for extraction and detection of analytes, determination of partition coefficient of chemicals, and many other droplet-based applications.

2. Experimental Section

2.1. Assembly of Flow Mixing Parts

The composition of the bulk solution was tuned by continuously mixing various solutions A_i at different flow rates. To achieve continuous mixing, each syringe containing different compositions of solution A was introduced into a passive mixer (polyether ether ketone manifold assembly 5 port, IDEX). Each stream was connected to a check valve (IDEX) to prevent backflow of the solutions. Unused parts were tightly sealed with paraffin film to prevent any potential leakage. **Figure 1** shows a schematic of the setup with three solutions A_i (i = 1, 2, 3) and one solution B. The mixture coming out of the flow distributor was introduced to a solvent exchange chamber containing a hydrophobized substrate (either Si wafer or glass) onto which surface nanodroplets were generated. A picture of the setup is shown in Figure S1, Supporting Information.

2.2. Preparation and Hydrophobilization of Substrates

The substrates (either Si wafer or a microscope glass slide) were rendered hydrophobic according to a previously reported method.[36] Briefly, a 1 cm $\times$ 2 cm Si wafer was treated

**ADVANCED
SCIENCE NEWS**

www.advancedsciencenews.com

**ADVANCED
MATERIALS
INTERFACES**

www.advmatinterfaces.de

with piranha solution (70% H_2SO_4 (Fisher Scientific) and 30% H_2O_2 (Fisher Scientific; v/v) at 70 °C for 15 min. Subsequently, the cleaned substrate was immersed in a 100 mL of *n*-hexane (Sigma-Aldrich) bath with 20 µL of octadecyltrichlorosilane (OTS) (Sigma-Aldrich) contained in a glass bottle. The glass bottle was tightly closed and left overnight for OTS coating. The coated substrate was then sonicated in ethanol and in water for 5 min each, and was dried by air blowing.

2.3. Preparation and Hydrophobization of Substrates

The multicomponent surface nanodroplets were formed by the solvent exchange method taking place on the hydrophobized substrate inside a flow chamber. The flow chamber consisted of a base plate with an inlet and an outlet. On top of the base plate, a silicon rubber spacer was placed which was subsequently covered with a top plate to create a channel. In the middle of the silicon rubber spacer, a piece of hydrophobized substrate was placed (see Figure S2, Supporting Information, for a detailed schematic of the flow chamber). To form the multicomponent droplets, the solutions A_i ($i = 1, 2, 3$) were injected at different volumetric flow rate ratios and mixed in the passive mixer and in the tubing prior to being introduced into the solvent exchange chamber. Subsequently, water was introduced as solution B into the solvent exchange chamber replacing the mixture of various solutions A. Although all the streams including solutions A_i ($i = 1, 2, 3$) and solution B were injected into the chamber through the passive mixer, no back-flow was observed due to the check valves placed in between each syringe and the passive mixer.

The continuous mixing setup enabled formation of multicomponent surface nanodroplets by mixing different solutions A_i prior to being injected into the solvent exchange chamber. The setup included a passive mixer with 5 inlets on the same place and one outlet placed vertically (Figure 1). Between the passive mixer and each syringe, a check valve was placed to prevent any potential contamination of the streams by potential back-flow of the mixture. When multiple solutions A_i were introduced into the passive mixer, they were mixed and the mixture flows through a 20 cm-long tube before being introduced into the solvent exchange chamber. At this stage, both the passive mixer and the tube ensured mixing of the various solutions A_i before the bulk mixture entered the solvent exchange chamber. Solution B was subsequently introduced into the solvent exchange chamber and replaced the solution A mixture to form the surface nanodroplets.

2.4. Image Acquisition and Analysis of Droplet Size

The fluorescence images of the surface nanodroplets were obtained using a fluorescence microscope (Nikon Eclipse Ni-U). The droplets were observed under green light, and the acquired images were processed and analyzed using a self-written python code. Using the code, the droplets were isolated from the background image by creating a mask after thresholding the entire image. Average fluorescence signal was calculated for each droplet.

3. Results and Discussion

3.1. Cycle and Repeatability of Droplet Formation by the Continuous Mixing Setup

The continuous flow-in system shown here employs a 5-way flow distributor as a passive mixer to combine multiple streams of solution A_i into a final mixture prior to being injected into the solvent exchange chamber. As the flow distributor has five ports, it can take up to three different solution A (A_1, A_2, A_3) and one solution B. The port on the center of the unit is used for the outflowing mixture. The advantage of the setup is that it is certainly possible to add more streams of solution A_i ($i = 4, 5, 6,...$) with other types of oils simply by replacing the flow distributor with inlet ports. In addition, 3D printing can equally be employed to customize the design of such units as the resolution of 3D printing technology has advanced enough to enable printing of microfluidic channels.[42]

Using the continuous flow-in system, single component surface nanodroplets were formed repeatedly as shown in **Figure 2**. As only one type of solution A was used, the other inlet ports of the fluid distributor were sealed with paraffin film. The droplets were visualized by doping the solution A with 1 µM of Nile red fluorescent dye. Repeated and reliable formation of droplets was easily achieved using the continuous mixing setup. As the solvent exchange was performed for three consecutive cycles, the process of droplet formation, dissolution, and re-formation could be clearly observed. During each cycle, the droplets were completely dissolved when fresh solution A entered the fluid chamber and new droplets were formed again once fresh solution B replaced solution A. The droplets formed during each cycle were similar in size as shown in the fluorescence images at t = 182, 261, and 778 s in Figure 2a and the size distribution plot in Figure 2b. Most of the droplets were between 7.5 µm and 10 µm in radius. The average fluorescent intensity of the droplets formed in each cycle was similar, indicating that the composition of the droplets formed between each cycle is also similar (Figure 2c).

Fast, reliable, and repeatable formation of surface nanodroplets is highly advantageous as it may be used for high throughput chemical analysis studies such as determination of partition coefficient of an unknown analyte,[9] or finding the optimal droplet composition in case of multicomponent systems. As shown in Figure 2a,b, droplets can be reliably obtained within 2–2.5 min. When combined with automated fluid delivery systems, we expect the setup demonstrated here will be capable of rapidly collecting a large amount of data.

The size of the droplets may be varied by the Peclét (*Pe*) number rate as shown in **Figure 3**a defined as $Pe = Q/wD$ where Q is the flow rate, w is the width of the channel, and D is the diffusion coefficient of oil in water. In our previous works,[36,43] we have shown that the final droplet volume scales with *Pe* due to a concentration gradient of oil formed as a result of an oversaturation pulse during the solvent exchange. In accordance with the previous results, the droplet size increased with *Pe*. However, at a very high *Pe*, the droplet size was non-uniform with large droplets (i.e., droplet radius > 50 µm) being formed together with small droplets (i.e., droplet radius < 5 µm). This is potentially due to the fact
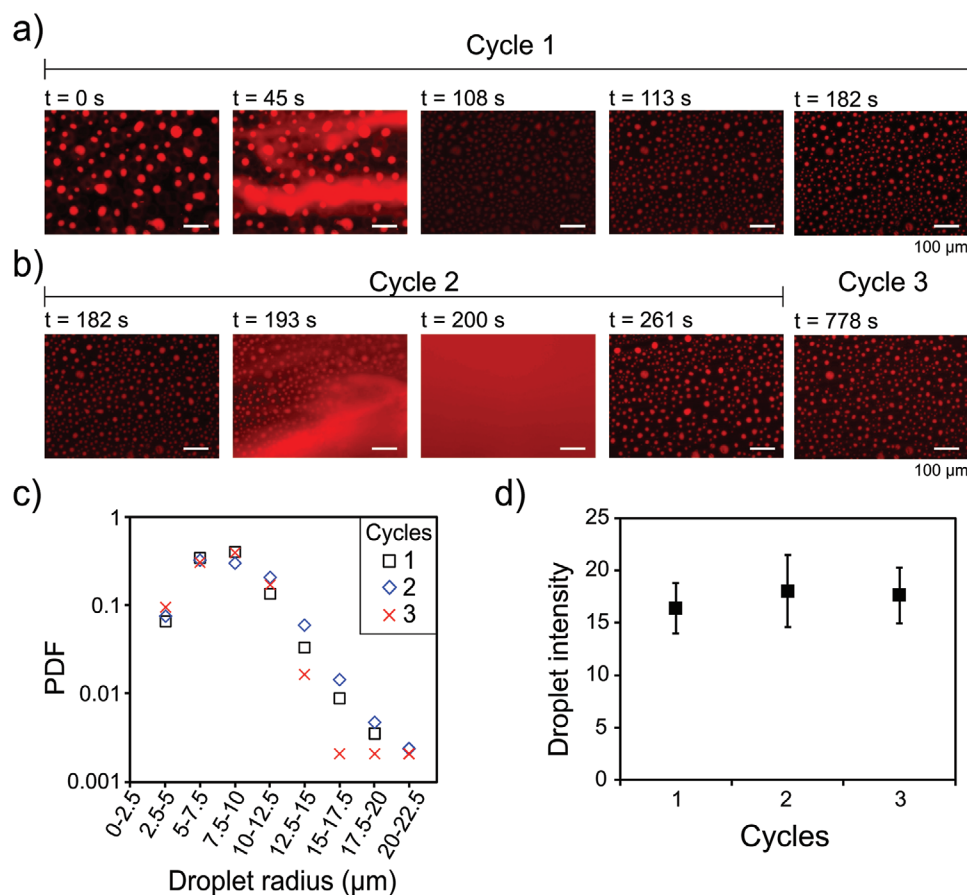
Figure 2. Time-lapse fluorescence images of surface nanodroplets formed over a) the first cycle and b) two consecutive cycles. For each cycle, the droplets are formed, dissolved when fresh solution A enters, and formed again as fresh solution B replaces solution A. c) Probability distribution function (PDF) of droplet sizes and d) average fluorescence intensities of droplets formed over the three consecutive cycles of solvent exchange.
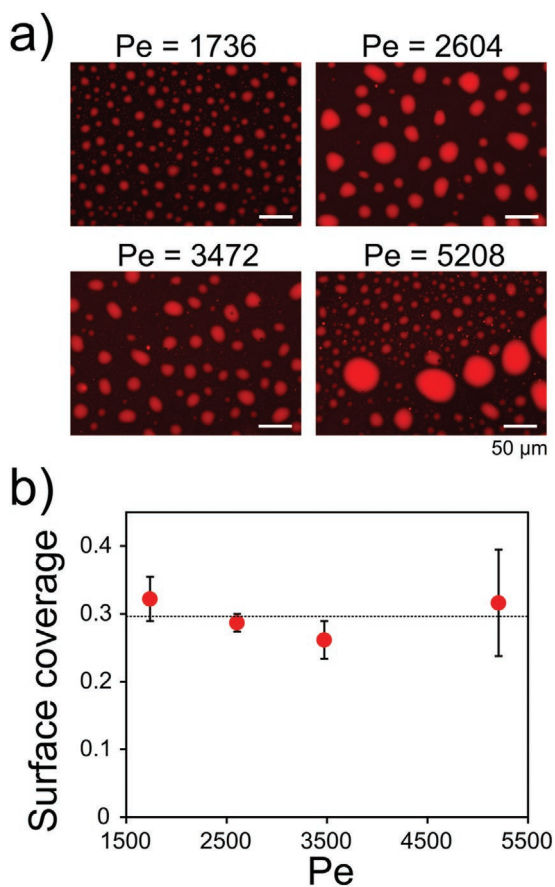
that at $Pe \approx 5208$, also Reynolds (Re) number is large ($\approx 9 \gg 1$), which may cause some droplets to be advected and merged with each other due to the higher inertia of solution B. Similar observations were reported earlier.[44] Although not shown here, the final droplet volume is also influenced by the channel height, the type of oil, and the composition of the initial mixture as shown in detail in our previous work.[36,43] The surface coverage of the droplets (Figure 3b) remained constant at ≈30% even as Pe increased, which is close to what was observed previously.[45]

3.2. Formation of Binary Droplets with Various Compositions

We now show the formation of binary droplets using the continuous mixing setup. A solution of 1-octanol in ethanol (solution A_1) was mixed with a solution of decane in ethanol (solution A_2). Both solutions were injected into the solvent exchange chamber. Here, the check valve placed between each syringe and the flow distributor prevents contamination of the solutions by blocking back-flow. Once the mixture of solution A_1 and A_2 fill the flow chamber, solution B was subsequently injected to form the binary surface nanodroplets composed of 1-octanol and decane.

The composition of the binary droplets can be determined using the phase diagram. **Figure 4**a shows the ternary phase diagram for water, ethanol, and oil, that is, 1-octanol or decane. The green and red lines indicate the phase boundaries for the ternary mixture involving decane and 1-octanol, respectively, constructed using phase equilibrium data.[46,47] On the phase diagram, a dilution line can be drawn from the point indicating the composition of solution A to that indicating the composition of solution B which is 100 mol% water. In this work, two different composition sets of solution A were tested: 2 mol%, indicated by the dotted line, and 5 mol%, indicated by the black solid line.

During solvent exchange, as solution B replaces A_1 and A_2, the composition in the mixing zone between solutions A_i ($i = 1, 2$) and B in the chamber passes through the Ouzo region in the phase diagram. Therefore, it was recently shown that the area between the dilution line and the phase boundary indicates the oversaturation level of the oil, and the composition of a multicomponent surface nanodroplet could be predicted based the ratios of the areas, and the composition in the bulk mixture of different solutions A_i can be correlated to the composition of the droplet.[9,48] As shown in Figure 4a, the areas between dilution lines and phase boundary for octanol and decane are not the same suggesting that the bulk mixture composition and

Figure 3. a) Fluorescence images showing the droplets formed at different Pe. Droplet size increases with Pe. b) Surface coverage of droplets at different Pe. The surface coverage remains nearly constant at $\approx 30\%$ for various Pe.

molar percentage of both octanol and decane in solutions A_1 and A_2, respectively, were kept the same at either 5 or 2 mol%. However, as the composition of the binary droplets is not the same as that of the bulk mixture, fluorescent Nile red dye was added only to the solution A_1 containing octanol. Nile red is a solvatochromic dye that emits fluorescence at different wavelengths.[49] Depending on the solvent at which it is dissolved in, Nile red can exhibit a positive red shift in the emission spectrum due to solvatochromatic effects[50] Therefore, the fluorescence signal from Nile red in the binary droplets is indicative of the relative amount of octanol to that of decane in the droplets. **Figure 5**a shows a series of fluorescence images with various octanol to total oil ratios ($r_{oct/(oct+dec)}$). The fluorescence intensity is highest when the droplet is only composed of octanol. However, the intensity sharply decreases as decane is added. At $r_{oct/(oct+dec)} = 0.5$, the intensity of the droplets is already quite low that the droplets are hardly visible. The situation is the same for the 2 mol% case; a sharp decay in fluorescence intensity is observed as the proportion of decane in the binary droplet is increased.

The average normalized fluorescence intensities of the binary droplets with $r_{oct/(oct+dec)}$ ranging between 0.5 to 1.0 were measured and plotted as shown by the red dots in Figure 5b for 5 mol%. In the same plot, calibration data obtained by bulk mixing the solutions A_i were also plotted as blue dots. The calibration data were obtained by first mixing both solutions A_1 and A_2 at various volume ratios such that the resulting mixture contained the same amount of octanol in the bulk. Both the data agree well with each other indicating that the solutions A_1 and A_2 mix well in the continuous mixer setup. Had incomplete mixing occurred, the fluorescence intensities of the binary droplets formed by bulk mixing and continuous mixing would have been different.

More importantly, it is clearly shown in Figure 5b that the normalized fluorescence intensity data of the binary droplets are in excellent agreement with the theoretical calculations obtained from the phase diagram indicated by the black solid line. Therefore, it is possible to predict the composition of the binary droplet from the bulk mixture composition or from the ratio of volumetric flow rates of solutions A_1 and A_2. Similarly, when the initial molar content of octanol and decane were
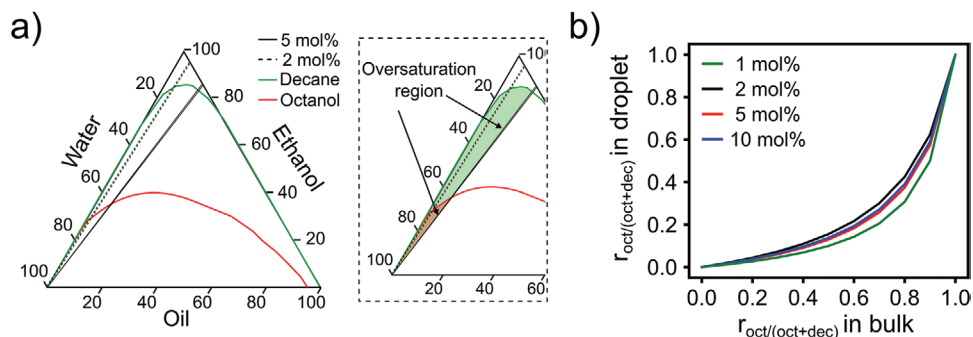
the droplet composition are not linearly related. In fact, when ratios of octanol to total oil amount in the bulk and in droplet are plotted, the two clearly exhibit a non-linear trend as shown in Figure 4b.

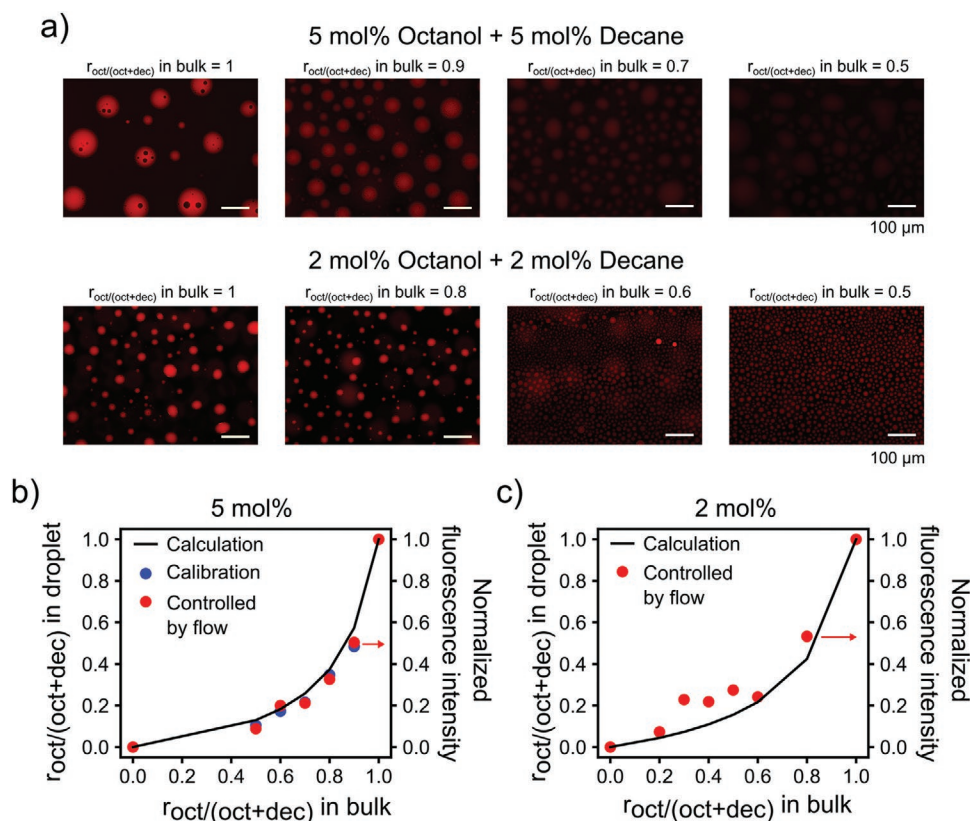Binary surface nanodroplet composed of octanol and decane were formed using the continuous mixer setup. The initial

Figure 4. a) Ternary phase diagram of water-ethanol-octanol or decane mixture. Green and red lines are the phase boundaries of the mixture when the oil is decane and octanol, respectively. Black solid and dotted lines are the dilution paths connecting the initial mixture to water. The zoomed in image shows the oversaturation region for 5 mol% octanol and 5 mol% decane cases. b) Plot showing $r_{oct/(oct+dec)}$ values in the bulk mixture and in the droplet. The $r_{oct/(oct+dec)}$ represent the proportions of octanol in the droplet and the values have been calculated from the areas between dilution path and phase boundaries.

**ADVANCED
SCIENCE NEWS**
www.advancedsciencenews.com

**ADVANCED
MATERIALS
INTERFACES**
www.advmatinterfaces.de

Figure 5. a) Fluorescence images showing binary droplets formed with various $r_{oct/(oct+dec)}$ in the bulk mixture for initial octanol and decane concentrations of 5 and 2 mol%. b) Plot comparing the average fluorescence intensities of the droplets formed with initial octanol and decane concentration of 5 mol% for various $r_{oct/(oct+dec)}$ in the bulk mixture to the calculated values of $r_{oct/(oct+dec)}$ in the droplet. Calibration data obtained by batch mixing are also shown as comparison. c) Plot showing the same as (b) but with initial octanol and decane concentration of 2 mol%.

reduced to 2 mol%, weaker fluorescence was observed for the binary droplets with lower $r_{oct/(oct+dec)}$, that is, with a higher proportion of decane.
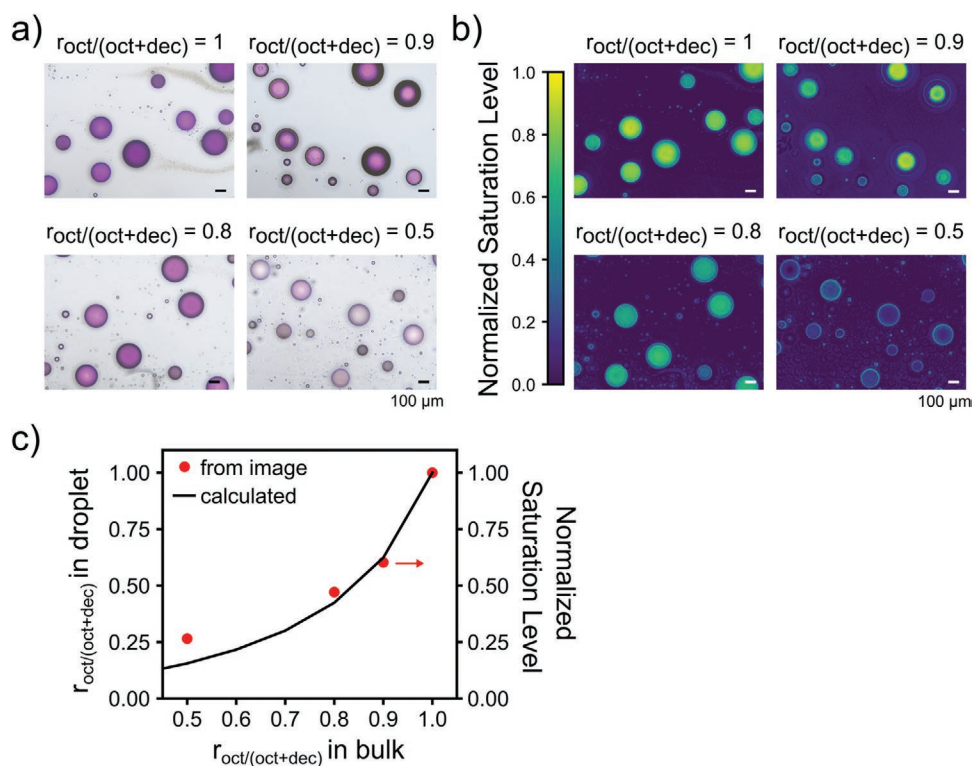
The solvatochromic effect of Nile red also enables colorimetric determination of octanol composition in the binary droplet. As shown in **Figure 6**, a purely octanol droplet shows a strong purple color which fades as the proportion of decane in the binary droplet increases. The bright field microscopy images can be converted to hue-saturation-value color space[51] and the normalized color saturation level of the droplets can be obtained (Figure 6b). As a result, the normalized saturation values for droplets of different octanol/decane ratios agree well with theoretical prediction. However, below $r_{oct/(oct+dec)}$ in bulk of 0.5, the color of binary droplet is too weak to be analyzed.

3.3. Formation of Ternary Droplets with Various Compositions

The advantage of the continuous mixer setup is that additional oil components can be added at will simply by introducing yet another solution A_i ($i = 3$) containing an additional oil. Here, we injected 2 mol% of toluene in ethanol as solution A_3 and formed octanol/decane/toluene droplets. **Figure 7**a shows fluorescence images of ternary droplets with compositions of Octanol (O)/Decane (D)/Toluene (T) ratios of O/D/T = 1.0/0.0/0.0, 0.5/0.5/0.0, 0.33/0.33/0.33 and 0.5/0.0/0.5 (in volumetric

ratios). The ternary droplets are brightest when they are 100% octanol and subsequently decreases as the proportions of decane and toluene increase. However, it is worth to note that the average intensities of the ternary droplets with composition O/D/T = 0.5/0.5/0.0 and with composition O/D/T = 0.5/0.0/0.5 are similar to each other as shown in Figure 7b. The similarities in fluorescence intensities suggest that the proportion of octanol in both cases is also similar, but it is not possible to determine either the amounts of toluene and/or decane in the droplets.

Additionally, as shown in Figure 7b, theoretical calculation based on the oversaturation region obtained from the phase diagrams is also not in agreement with the fluorescence intensities, in contrast to the case of binary droplets. In fact, the ratio $r_{oct/(oct+dec+tol)}$ in the droplet for O/D/T = 0.5/0.5/0 case is quite different from $r_{oct/(oct+dec+tol)}$ in droplet for O/D/T = 0.5/0.0/0.5. Despite the fact that $r_{oct/(oct+dec+tol)}$ in the bulk for both cases is 0.5, the r values in the droplets are different due to the difference in oversaturation areas. As shown in Figure S3, Supporting Information, the phase boundary for toluene sits between that of octanol and decane. As the area bounded by the dilution line and each phase boundary represents the amount of each component in the droplet, the same ratio $r_{oct/(oct+dec+tol)}$ in the bulk in general does not mean the same ratio $r_{oct/(oct+dec+tol)}$ in droplet. Moreover, extraction of decane and toluene by octanol during mixing of the three solutions A_i ($i = 1, 2, 3$) can influence the

ADVANCED
SCIENCE NEWS
www.advancedsciencenews.com

ADVANCED
MATERIALS
INTERFACES
www.advmatinterfaces.de

Figure 6. a) Bright field microscopy images and b) processed images of octanol/decane binary droplets with $r_{oct/(oct+dec)}$ in droplet of 1, 0.9, 0.8, and 0.5. The processed images show a measure of the color saturation in hue-saturation value (HSV) color space. As evidenced by the microscopy images, the purple color of the droplets fades away as the proportion of decane in the droplets increases. In the HSV color space, the droplet decolorizes as decane content increases. c) Normalized saturation values (red dots) and calculated $r_{oct/(oct+dec)}$ in droplet (black solid line) plotted against $r_{oct/(oct+dec)}$ in bulk.

composition. The octanol-water partition coefficients of decane and toluene are ≈5 and 2–3, respectively.[52] Therefore, during solvent exchange, as the droplet nucleates on the substrate and begins to grow, decane and toluene molecules in the mixing zone can be extracted into the droplet.

4. Conclusion

In this work, we showed the formation of binary and ternary droplets with tunable composition using a continuous flow mixer setup. Streams of solutions A_i containing various oils are mixed
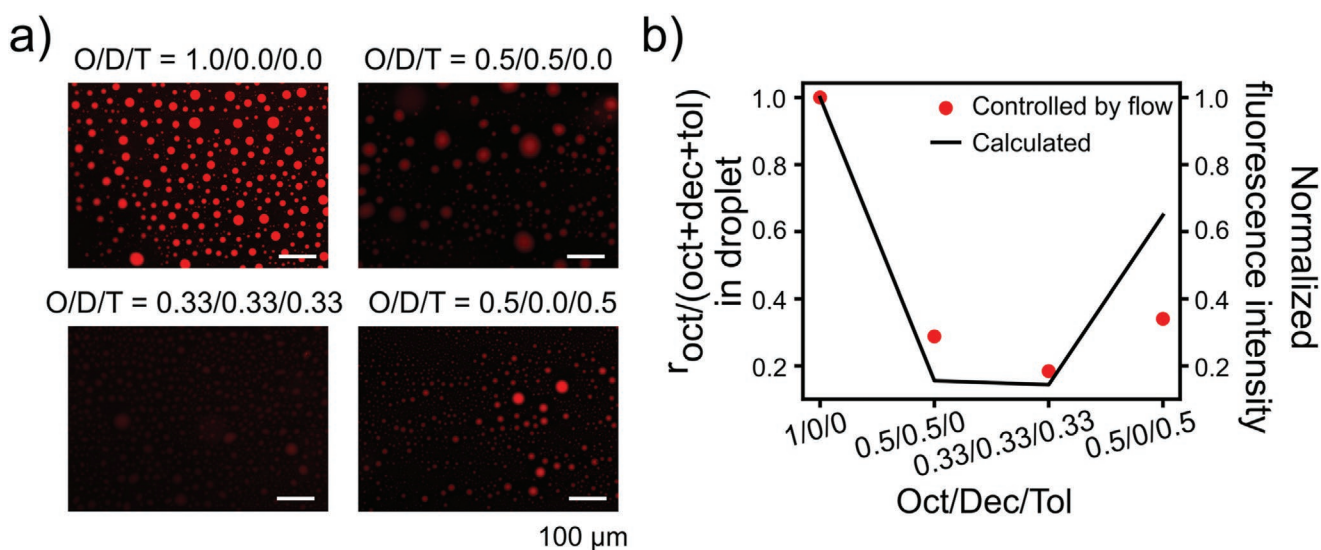
Figure 7. a) Fluorescence images of ternary droplets formed with octanol (O), decane (D), and toluene (T) at mole ratios of O/D/T = 1.0/0.0/0.0, 0.5/0.5/0.0, 0.5/0.0/0.5, and 0.33/0.33/0.33. b) Fluorescence intensity of the ternary droplets plotted with theoretical calculation of $r_{oct/(oct+dec+tol)}$ in droplet.

in a passive flow mixer after which the outcoming mixture is injected into the flow chamber where surface nanodroplets form. The compositions of the binary or ternary surface nanodroplets are controlled by the flow rate ratios of different streams of solutions A_i ($i = 1, 2, 3,...$), which have been confirmed to match with theoretical calculations based on the phase diagrams. Droplets can be formed within 2.5 min with high repeatability. The method shown here is not limited to water immiscible organic solvents, but can also be used to generate ionic liquid droplets that require two or more components or to form nanolenses consisting of various polymers. Therefore, the facilitated multicomponent droplet formation with tuneable composition is potentially applicable to a wide range of fields including platforms for ultrasensitive chemical detection, determination of partition coefficient of chemicals or synthesis of functional materials.

Supporting Information

Supporting Information is available from the Wiley Online Library or from the author.

Conflict of Interest

The authors declare no conflict of interest.

Data Availability Statement

Research data are not shared.

[1] Z. Wei, Y. Li, G. Cooks, X. Yan, *Annu. Rev. Phys. Chem.* **2020**, *71*, 31.
[2] R. M. Bain, S. Sathyamoorthi, R. N. Zare, *Angew. Chem.* **2017**, *129*, 15279.
[3] H. Song, D. L. Chen, R. F. Ismagilov, *Angew. Chem., Int. Ed.* **2006**, *45*, 7336.
[4] S. Tang, T. Qi, P. D. Ansah, J. C. N. Fouemina, W. Shen, C. Basheer, H. K. Lee, *Trends Anal. Chem.* **2018**, *108*, 306.
[5] L. Zhang, J. Sun, H. He, Y. Huang, H. Shi, W. Chen, *Lab Chip* **2021**, *21*, 2217.
[6] H. Haidas, S. Bachler, M. Köhler, L. M. Blank, R. Zenobi, P. S. Dittrich, *Anal. Chem.* **2019**, *3*, 2066.
[7] H. N. Joensson, H. A. Svahn, *Angew. Chem., Int. Ed.* **2012**, *51*, 12176.
[8] A. Kulesa, J. Kehe, J. E. Hurtado, P. Tawde, P. C. Blainey, *Proc. Natl. Acad. Sci. U. S. A.* **2018**, *115*, 6685.
[9] M. Li, B. Dyett, H. Yu, V. Bansal, X. Zhang, *Small* **2019**, *15*, 1804683.
[10] S. Liao, X. Tao, Y. Ju, J. Feng, W. Du, Y. Wang, *ACS Appl. Mater. Interfaces* **2017**, *9*, 43545.
[11] A. Frenz, L. El Harrak, M. Pauly, S. Bégin-Colin, A. D. Griffiths, J. C. Baret, *Angew. Chem., Int. Ed.* **2008**, *47*, 6817.
[12] Y. J. Hwang, C. W. Coley, M. Abolhasani, A. L. Marzinzik, G. Koch, C. Spanka, H. Lehmann, K. F. Jensen, *Chem. Commun.* **2017**, *53*, 6649.
[13] I. Liascukiene, M. Jehannin, J. Lautru, R. Podor, S. Charton, F. Testard, *J. Phys. Chem. C* **2021**, *125*, 9428.
[14] H. Xiong, J. K. Lee, R. N. Zare, W. Min, *J. Phys. Chem. B* **2020**, *124*, 9938.
[15] M. Li, B. Dyett, X. Zhang, *Anal. Chem.* **2019**, *16*, 10371.
[16] D. Lohse, X. Zhang, *Rev. Mod. Phys.* **2015**, *87*, 981.
[17] J. Qian, G. F. Arends, X. Zhang, *Langmuir* **2019**, *35*, 12583.
[18] J. Qian, D. Yamada, Z. Wei, R. Yukisada, Y. Tagawa, J. M. Shaw, X. Zhang, *Adv. Mater. Technol.* **2020**, *5*, 1900740.
[19] Z. Li, A. Kiyama, H. Zeng, D. Lohse, X. Zhang, *Lab Chip* **2020**, *20*, 2965.
[20] L. Hamadeh, S. Imran, M. Bencsik, G. R. Sharpe, M. A. Johnson, D. J. Fairhurst, *Sci. Rep.* **2020**, *10*, 3313.
[21] Z. Zhou, X. Li, R. N. Zare, *ACS Cent. Sci.* **2017**, *3*, 1337.
[22] S. Jiang, J. Noh, C. Park, A. D. Smith, N. L. Abbott, V. M. Zavala, *Analyst* **2021**, *146*, 1224.
[23] J. Zhu, Q. Wang, M. Li, L. Ren, B. Zheng, X. Zou, *Anal. Methods* **2017**, *9*, 1855.
[24] X. Wang, Y. Wang, X. Zou, Y. Cao, *Anal. Methods* **2014**, *6*, 2384.
[25] G. D. Bozyiğit, M. F. Ayyildiz, D. S. Chormey, G. O. Engin, S. Bakirdere, *Environ. Toxicol. Chem.* **2021**, *40*, 1570.
[26] H. Tan, C. Diddens, P. Lv, J. G. M. Kuerten, X. Zhang, D. Lohse, *Proc. Natl. Acad. Sci. U. S. A.* **2016**, *113*, 8642.
[27] H. Tan, C. Diddens, M. Versluis, H. J. Butt, D. Lohse, X. Zhang, *Soft Matter* **2017**, *13*, 2749.
[28] D. Lohse, X. Zhang, *Nat. Rev. Phys.* **2020**, *2*, 426.
[29] I. F. Guha, S. Anand, K. K. Varanasi, *Nat. Commun.* **2017**, *8*, 1371.
[30] R. Zhang, W. Liao, Y. Wang, Y. Wang, D. Ian Wilson, S. M. Clarke, Z. Yang, *J. Colloid Interface Sci.* **2021**, *584*, 738.
[31] S. Y. Teh, R. Lin, L. H. Hung, A. P. Lee, *Lab Chip* **2008**, *8*, 198.
[32] X. Casadevall i Solvas, A. deMello, *Chem. Commun.* **2011**, *47*, 1936.
[33] E. M. Payne, D. A. Holland-Moritz, S. Sun, R. T. Kennedy, *Lab Chip* **2020**, *20*, 2247.
[34] H. Song, J. D. Tice, R. F. Ismagilov, *Angew. Chem., Int. Ed.* **2003**, *42*, 768.
[35] S. Sohrabi, N. Kassir, M. K. Moraveji, *RSC Adv.* **2020**, *10*, 27560.
[36] X. Zhang, Z. Lu, H. Tan, L. Bao, Y. He, C. Sun, D. Lohse, *Proc. Natl. Acad. Sci. U. S. A.* **2015**, *112*, 9253.
[37] M. Li, L. Bao, H. Yu, X. Zhang, *J. Phys. Chem. C* **2018**, *122*, 8647.
[38] M. Li, H. Yu, L. Bao, B. Dyett, X. Zhang, *J. Colloid Interface Sci.* **2019**, *543*, 164.
[39] S. A. Vitale, J. L. Katz, *Langmuir* **2003**, *19*, 4105.
[40] S. Prévost, S. Krickl, S. Marčelja, W. Kunz, T. Zemb, I. Grillo, *Langmuir* **2021**, *37*, 3817.
[41] M. Li, R. Cao, B. Dyett, X. Zhang, *Small* **2020**, *16*, 2004162.
[42] A. V. Nielson, M. J. Beauchamp, G. P. Nordin, A. T. Woolley, *Annu. Rev. Anal. Chem.* **2020**, *13*, 45.
[43] H. Yu, S. Maheshwari, J. Zhu, D. Lohse, X. Zhang, *Lab Chip* **2017**, *17*, 1496.
[44] B. Zeng, Y. Wang, X. Zhang, D. Lohse, *J. Phys. Chem. C* **2019**, *123*, 5571.
[45] C. Xu, H. Yu, S. Peng, Z. Lu, L. Lei, D. Lohse, X. Zhang, *Soft Matter* **2017**, *13*, 937.
[46] A. Arce, A. Blanco, P. Souza, I. Vidal, *J. Chem. Eng. Data* **1994**, *39*, 378.
[47] A. Skrzecz, D. Shaw, A. Maczynski, *J. Phys. Chem. Ref. Data* **1999**, *28*, 983.
[48] Z. Lu, S. Peng, X. Zhang, *Langmuir* **2016**, *32*, 1700.
[49] S. Kalathimekkad, J. Missinne, D. Schaubroeck, R. Mandamparambil, G. Van Steenberg, *IEEE Sens. J.* **2015**, *15*, 76.
[50] A. K. Dutta, K. Kamada, K. Ohta, *J. Photochem. Photobiol. A* **1996**, *93*, 57.
[51] K. Cantrell, M. M. Erenas, I. de Orbe-Payá, L. F. Capitán-Vallvey, *Anal. Chem.* **2010**, *82*, 531.
[52] J. Sangster, *J. Phys. Chem. Ref. Data* **1989**, *18*, 1111.